J Solid State Electrochem (2006) 10: 1–9
DOI 10.1007/s10008-004-0638-2

ORIGINAL PAPER

Jesús Santos-Peña · Patrick Soudan
Carlos Otero Areán · Gemma Turnes Palomino
Sylvain Franger

Electrochemical properties of mesoporous iron phosphate in lithium batteries

Received: 28 September 2004 / Revised: 11 October 2004 / Accepted: 19 November 2004 / Published online: 18 January 2005

Abstract Mesoporous iron phosphate containing CTAB as templating agent was synthesized and characterized by means of X-ray diffraction, Fourier transform infrared spectroscopy and TGA techniques. The mesoporous material shows a highly ordered structure, that collapses when submitted to extraction with acetate ions. The treatment of the exchanged samples at 573 K under nitrogen atmosphere leads to amorphous phases with an electrochemical behaviour typical of carbon-coated iron phosphate electrodes. The existence of this coating, proceeding from incomplete pyrolysis of the organic exchange agent, enhances the electronic properties of the system, as evidenced by galvanostatic experiments and impedance spectroscopy measurements.

Keywords Iron phosphates · Mesoporous materials · Lithium ion batteries · Positive electrodes · Electrochemical impedance spectroscopy

Introduction

The search for positive electrodes, competitive with $LiCoO_2$ and stabilised $LiNiO_2$ has arosen much attention on lithium iron phosphate [1–3], an olivine structure that develops a voltage plateau at 3.5 V versus lithium, and provides a capacity as high as 170 mAh g^{-1}, but shows poor electronic properties. When $LiFePO_4$ is totally charged at 4.0 V, $FePO_4$ with an heterosite structure is obtained [3], where Fe(II) is octahedrally coordinated by oxygen proceeding from the PO_4^{3-} polyanion. In fact, this octahedral coordination is responsible for the topotactic character of the reaction involving the Fe(III)/Fe(II) redox couple, during the charge/discharge cycles. After the pioneering study of Prosini et al. [4], a wide series of lithium free iron phosphates have been examined for electrochemical purposes by the groups of Whittingham [3, 5, 6] and Masquelier [7, 8]. The main observation is that iron phosphates, $FePO_4{\cdot}xH_2O$ ($0 < x < 3.4$), containing tetrahedral iron (III), behave poorly in lithium cells, due to the instability of tetrahedral iron (II) at the end of the discharge. Consequently, the structures tridimite, α-quartz and β-quartz of anhydrous or hydrated phosphates provide a bad performance [5–7]. Other feature largely investigated is the role of water content in the iron phosphate composition. Amorphous $FePO_4{\cdot}2H_2O$ can react with lithium in conditions close to equilibrium to yield $Li_{1.0}FePO_4{\cdot}2H_2O$ [4] or with non-steady techniques to yield $Li_{0.7}FePO_4{\cdot}2H_2O$ [5]. Both its disordered nature and the presence of two coordinated water molecules account for this first capacity. Structural water seems to enhance the ionic conduction properties of the solid, solvating the lithium ions during the intercalation/deintercalation process. However, this amorphous phase is characterised by a capacity loss during the first charge [4–9]. Inherent to both types of materials, there is a lack of conductivity that leads to capacity fading by cycling. The ball-milling of the cathode powders with carbon or ruthenium oxide has been effective to increase the reactivity and cycling life of amorphous hydrated compound [7] and a crystalline anhydrous phase [8, 9], respectively.

In this work, we have approached the multiple issues of the iron phosphates under a new perspective, by studying the electrochemical properties of a mesoporous structure [10] constituted by amorphous walls of com-

J. Santos-Peña (✉) · C. O. Areán · G. T. Palomino
Departament de Quimica, Edifici Mateu Orfila,
Universitat de les Illes Balears,
07123 Palma de Mallorca, Spain
E-mail: vdqujsp0@uib.es
Tel.: +34-971-173389
Fax: +34-971-173426

P. Soudan
Laboratoire d'Electrochimie, Catalyse et Synthèse Organique,
UMR CNRS 7582, ISCSA, 2 rue Henri Dunant,
94320 Thiais, France

S. Franger
Laboratoire de Physico-Chimie de l'Etat Solide,
UMR CNRS 8648, ICMMO, Université Paris XI,
91405 Orsay, France

position close to $FePO_4{\cdot}2H_2O$. The study of this phase was investigated after the extraction of the surfactant agent by an exchange treatment, followed or not by calcination under different atmospheres at 573 K. Heating the samples at this temperature provokes the collapse of the structure, thus an increase in the disorder of the system and a decrease in the mesoporosity. Interesting results were provided by a material containing carbon in its structure obtained from an exchanged mesophase calcined under nitrogen atmosphere. The electrochemical properties of the different materials obtained from the mesoporous iron phosphate were compared with those of amorphous $FePO_4{\cdot}2H_2O$.

Materials and methods

Synthesis of the mesoporous iron phosphates and related materials

Mesoporous iron phosphate was prepared following the procedure of Guo et al. [10] modified by the use of CTAB in place of sodium laurylsulfate as surfactant. To a suspension of freshly prepared amorphous iron phosphate in water, HF is added with vigorous stirring. After the dissolution of iron phosphate, an aqueous solution of CTAB is added and the whole system is kept in stirring for 30 min. The system is then heated to 60 °C and held for 2.5 h. After cooling to room temperature, no precipitate was observed in contrast with that reported for the dodecylsulfate procedure. An increase of the pH solution from 2 to 10, promoted by the addition of 1 M TPAOH solution, led to the precipitation of a yellow solid. Then, the solid was recovered by centrifugation and repeatedly washed with water and acetone, yielding the mesoporous phosphate. Extraction of the surfactant was carried out by an ion exchange procedure by treating the previous freshly prepared sample with a 0.05 M ethanol solution of sodium acetate under continuous stirring. After extraction, the solid was repeatedly submitted to centrifugation, washed with ethanol, and finally let to dry in air. The extraction of CTAB was checked by thermogravimetric and FTIR analysis. The exchanged samples are so called samples A.

For electrochemical purposes, two additional samples were prepared by heating the exchanged mesophase at 573 K respectively under air (sample B, light yellow colour) or nitrogen (sample C, black colour).

Characterisation of the samples

X-ray diffraction (XRD) patterns were recorded on a Siemens D5000 X-ray diffractometer, using CuK_α radiation ($\lambda = 1.54059$ Å) and a graphite monochromator.

Thermogravimetric analysis was carried out in a SDT 2960 simultaneous DSC-TGA instrument, with a balance sensitivity of 0.1 μg (±1%) and a ΔT sensitivity of 0.001 °C, with Pt–Pt/13%Rh type R thermocouples. Samples were heated at 10 K/min from room temperature to 800 °C, under a 120 ml min^{-1} oxygen flow.

Scanning electron microscope images were obtained on a Leica Stereoscan microscope with an energy dispersive X-rays (EDX) analyser coupled. Iron and phosphorus content in our samples were obtained by using this analyser. Transmission electron micrographs were obtained with a Hitachi H600 instrument operating at 75 kV and with an EDX analyser coupled.

FTIR spectra on KBr-based pellets, were collected with a Bruker IFS66 instrument used in the transmittance mode. Spectra were recorded at 4 cm^{-1} intervals over the 4,000–400 cm^{-1} range.

The electrochemical characteristics were determined with either two-electrode (for cycling) or three-electrode (for impedance spectroscopy) electrochemical cells.

The working electrode consisted of a stainless steel grid on which the cathodic material was pressed. The cathode was made of a mixture of active material (80% wt) with graphite (7.5% wt), acetylene black (7.5% wt) and PTFE (5% wt). The mixture is pressed on to a stainless-steel grid, with a geometric area of 1 cm^2. The electrolyte used was 1 M $LiClO_4$ in propylene carbonate. Propylene carbonate, double-distilled, was obtained from Fluka and used as received. Anhydrous lithium perchlorate was dried under vacuum at 200 °C for 12 h.

Galvanostatic cycling experiments were performed using two-electrode Swagelock-type stainless steel cells with Whatman GF/C glass microfibre filter discs as separator. Cycles were performed using a MacPile II (BioLogic) potentiostat connected to an Imac computer. Working electrodes were cycled in the potential window 2–4 V versus the lithium counter electrode (consisted of a lithium foil) also used as reference. The discharge-charge rate was C/20 for 1 Li/P.

Impedance measurements were performed with three-electrode electrochemical cells in which the reference electrode is a lithium wire in a separate compartment and counter electrode consisted of a gold wire directly immersed in the electrolyte solution, close to the working electrode. The experiments were made with a potentiostat EGG PAR 273 A coupled with a 1255 Schlumberger Frequency Response Analyser in the frequency range 10^4 to 10^{-3} Hz The excitation signal was 14 mV peak to peak. The equilibrium potential was considered to be reached when the drift in open-circuit voltage remained less than 1 mV h^{-1}. Fitting of the impedance diagramms were realized with Zplot software from Scribner.

Results and discussion

XRD measurements

The diffraction patterns of the two ordered mesophases obtained (as synthesized product and sample A) are shown in Fig. 1. The amorphous nature of the iron phosphate used as precursor contrasts with the ordered

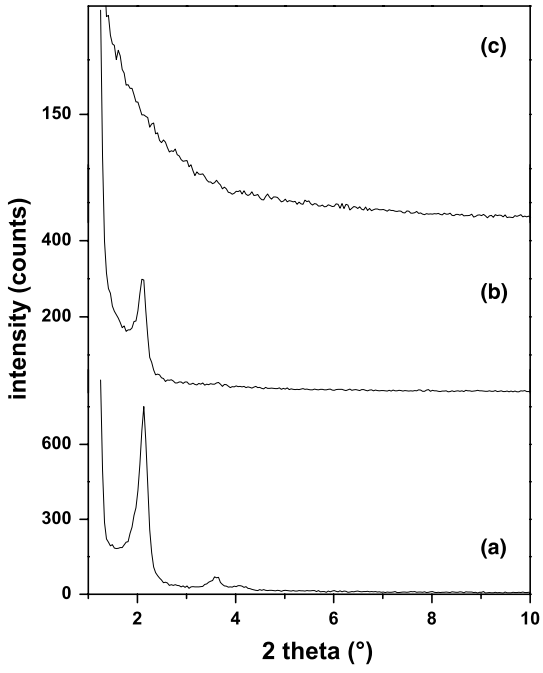

Fig. 1 XRD patterns of **a** as synthesized mesoporous iron phosphate, **b** sample A, **c** sample B

as-synthesised mesoporous material whose diffractogram (Fig. 1a) is characterised by three peaks at 2.1, 3.6, and 4.1°, corresponding to pore plan reflections. It is interesting to note that the mesophase obtained by using CTAB as template, is more ordered than that for sodium laurylsulfate template [10], which diffractogram only shows one peak at 2.4°. After exchange, the mesostructure partially collapses as the two latter diffraction peaks disappear and the basal peak intensity decreases (Fig.1b). Therefore, the stability of the as synthesized mesophase versus the extraction is lower than for the mesoporous iron phosphate obtained by Guo, which can be easily ascribed to the proved role of sulfate-based surfactants in obtaining highly stable non-siliceous mesophases.

The treatments at 573 K under air or nitrogen atmospheres of sample A led to an increased disorder in the pores distribution as shown in Fig. 1c. XRD patterns of samples B and C in a wide angle region (1.5–80°) (not shown therein) indicate than both samples are amorphous. Up to now, thermal stability of the mesoporous iron phosphate obtained by the laurylsulfate method has not been reported.

Infrared spectroscopic features

FTIR spectroscopy provided information about purity of the mesophases obtained. Figure 2 shows the infrared spectra of as synthesized mesophase and sample A. Spectrum of amorphous $FePO_4{\cdot}2H_2O$, (precursor of sample A), shown for comparison, consists of a broad band in the 3,600–2,500 cm^{-1} region and a peak at 1,630 cm^{-1} that can be ascribed to the presence of composition water, besides characteristic peaks at 1,060 cm^{-1} and 920 cm^{-1} [11]. Moreover, the lack of bands at 1,020, 990, 890 and 470 cm^{-1} discard the presence of γ-FeOOH, $Fe_3(PO_4)_2$, α-FeOOH and δ-FeOOH, respectively, in the precursor [12]. The presence of cetyltrimethylamonium group in the mesoporous material is checked in the Fig. 2b. Two intense peaks assigned to asymmetric (2,922 cm^{-1}) and symmetric (2,858 cm^{-1}) stretching vibrations of C–CH_2 in the methylene chains, are observed. Sharp bands in the region 1,450–1,500 cm^{-1} are attributed to the deformation of –CH_2– and –CH_3 of the incorporated surfactants. The weak band at 3,025 cm^{-1} is assigned to C–CH_3 asymmetric stretching and N–CH_3 symmetric stretching vibrations of solid surfactant. The existence of CH_2 vibrations at 2,858 cm^{-1} and 2,922 cm^{-1} indicates that the surfactant is present as micelles in the as-synthesized mesostructured iron phosphate [13, 14]. After exchanging (Fig. 2c), the infrared spectra is quite similar with that of amorphous $FePO_4{\cdot}2H_2O$ (Fig. 2a). In fact, the bands due to CTAB have disappeared and, again, water is present in this sample, yielding a broad band between 3,000 cm^{-1} and 3,700 cm^{-1} and a peak at 1,642 cm^{-1}, corresponding to O–H stretching and deformation vibrations. The position of these bands also reveals that the linking of these water molecules to the structure is not weak. Finally, the exchange process introduces a weak peak at 1,400 cm^{-1} that can be ascribed to the presence of a little amount of acetate [13].

Infrared spectra of sample B and sample C (not shown) confirmed the removal of exchange agent as the 1,400 cm^{-1} band has disappeared.

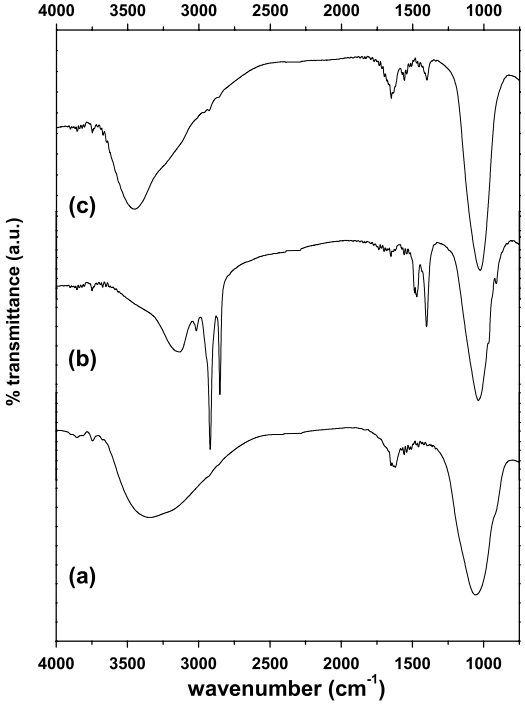

Fig. 2 FTIR spectra of **a** amorphous $FePO_4{\cdot}2H_2O$, **b** as synthesized mesoporous iron phosphate, **c** sample A

Thermogravimetric measurements

Figure 3 shows the thermograms of sample A and its amorphous precursor. For the amorphous phosphate, the TG curve shows a well defined weight loss between 323 K and 773 K, which is ascribed to elimination of crystallisation water. The total mass loss is 20.68%, which corresponds quite well to 2 mol of water for each mole of $FePO_4$ [5, 15, 16].

Thermogravimetric curve of as synthesized mesophase, shows three steps corresponding to the removal of water molecules (below 473 K), the desorption and decomposition of the surfactant (353–698 K) and the dehydroxylation of the surface and the removal of little residual surfactant (698–873 K). The three steps have been already identified for tin oxide mesoporous phase obtained by using CTAB as surfactant agent [14]. The composition of this phase, calculated on the basis of the weight loss is $FePO_4{\cdot}(CTAB)_{0.25}{\cdot}1.7H_2O$.

The absence of the CTAB in sample A is confirmed by recording the corresponding thermogram (Fig. 2c). Instead of the well defined weight loss in the 453–698 K region, we distinguish the shape decomposition of acetate groups (in agreement with infrared measurements) in the temperature region 423–623 K. Once acetate is decomposed, dehydroxylation of the surface takes place. However, overlapping of the different processes hinders the accurate determination of the sample A composition by thermogravimetric measurements. Besides that, we can remark that after exchange, the mesoporous solid seems to contain water molecules (in a first approximation, 2–3 mol of water per mol of $FePO_4$). The excess of water from the original phase can be associated to the reported hygroscopic character of some iron phosphates [7, 8].

On the basis that sample A seems to be a mesoporous variant of the amorphous $FePO_4{\cdot}2H_2O$, (this one of interest as positive electrode for lithium ion batteries), we have approached the study of its electrochemical application in lithium cells. The existence of pore channel system in sample A should facilitate the lithium diffusion in this system, if remaining sodium acetate does not hinder it. Samples B and C, namely amorphous anhydrous $FePO_4$ are also interesting as the remaining acetate groups are definitively absent in the network. However, the thermal treatment also implies the loss of pores ordering and mesoporosity in both samples, which hinder the lithium diffusion through these materials. For both samples B and C, water is released in the 323–473 K region, and corresponds to ca. 11% in weight, evidencing the hygroscopic behaviour of these solids [7, 8]. However, TG analysis (Fig. 3d.) shows for sample B a weight loss (10%) in the 473–723 K region, difficult to explain if we consider that acetate groups in both samples were removed during the treatment at 573 K.

Microscopy examinations

Figure 4 shows one scanning electron micrograph corresponding to amorphous $FePO_4{\cdot}2H_2O$. This material is composed of nanoparticles with size ranging between 40 nm and 80 nm and round shape. These results are in agreement with earlier reported products obtained from water solutions containing Fe(III) and $NH_4H_2PO_4$ [4, 15, 16]. TEM images have been obtained for samples A and B, of electrochemical interest, and are shown in

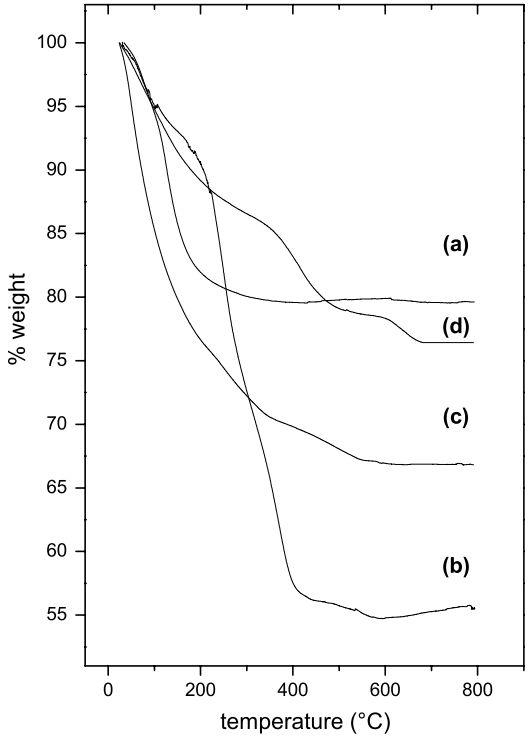

Fig. 3 Thermogravimetric analyses under air flow of **a** amorphous $FePO_4{\cdot}2H_2O$, **b** as synthesized mesoporous iron phosphate, **c** sample A, **d** sample B

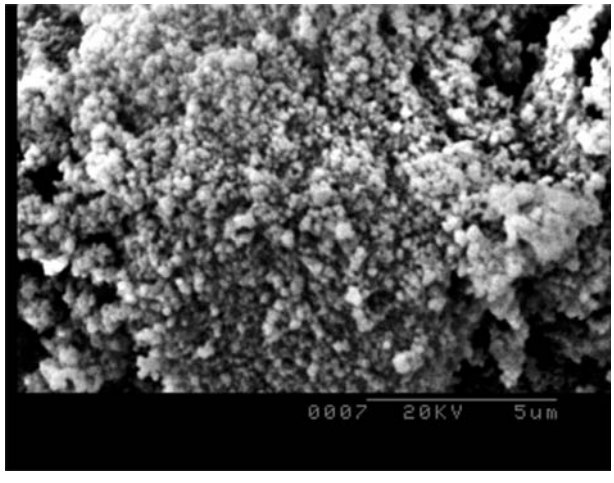

Fig. 4 Scanning electron microscope image of amorphous $FePO_4{\cdot}2H_2O$ obtained from precipitation of an iron nitrate solution with a NaH_2PO_4 solution

Fig. 5. The low resolution of the microscope hinders the observation of the sample A ordered pore structure. However, both images allow conclude that thermal treatment produces fractures in the mesostructure and discriminate the average size of the particles, which is below 90 nm.

Energy dispersive X-rays analyser coupled with the TEM instrument detected carbon and sodium in sample A, as sodium acetate proceeding from the extraction are retained in that structure. Samples B and C, obtained by thermal treatment at 573 K, still contain sodium in their compositions although no traces of carbon are detected. According to these features, sodium could be fixed to the pore $FePO_4$ walls as different oxide-entities for sample B and sample C. Moreover, sample C, black in colour, retained little and undetectable traces of carbon, proceeding from the incomplete pyrolysis of acetates under nitrogen atmosphere.

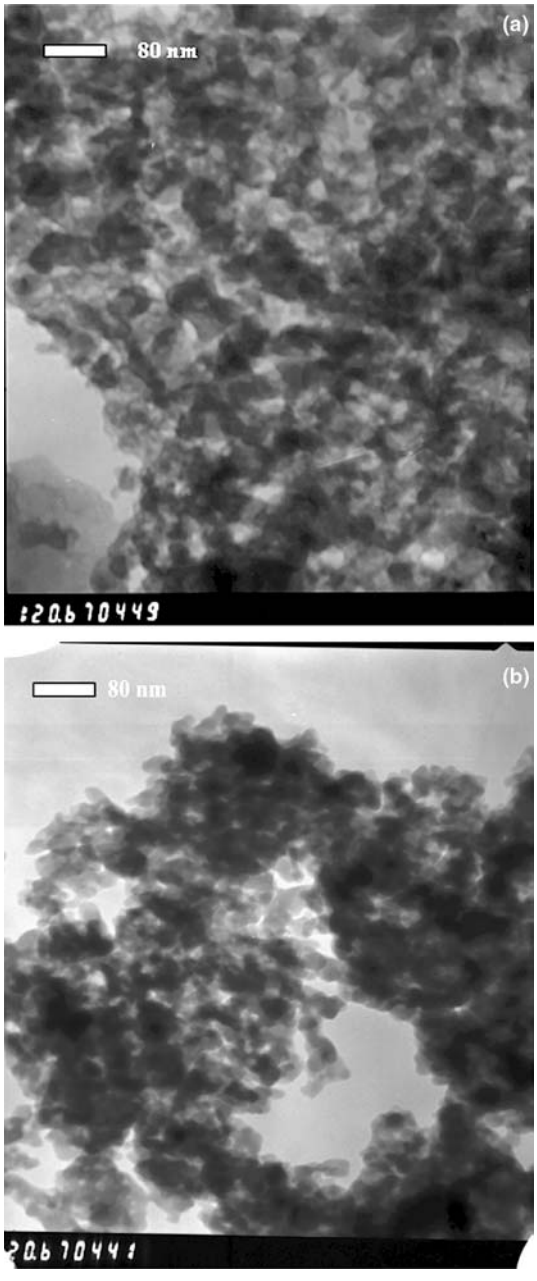

Fig. 5 TEM images of **a** sample A and **b** sample B

Electrochemical tests

Figure 6 shows the first cycles of the different samples studied in lithium cells with 1 M $LiClO_4$/PC electrolyte and under a C/20 regime discharge. Voltage range (4.0–2.0 V) was fixed according to the literature on these systems. The voltage-composition curve of a cell based on amorphous $FePO_4{\cdot}2H_2O$ (Fig. 6a) shows the typical S-type earlier reported by Prosini [4], Whittingham [5] and Masquelier [7], where a pseudoplateau at 3.0 V is evidenced before voltage quickly fades close to 2.0 V. This pseudoplateau is ascribed to the reversible reaction:

$$x\ Li + FePO_4 \rightarrow Li_xFePO_4 \quad (1)$$

It is noteworthy that our sample reacts in the first discharge with 0.65 F Li/mol $FePO_4{\cdot}2H_2O$, a value intermediate between those reported by Whittingham and Masquelier groups. As the procedure for the sample preparation is similar for the three groups, we believe that differences in the first discharge are mostly due to the preparation of the composite electrode. When sign of current is reversed, the cell polarizes ca. 1.0 V prior the development of a pseudoplateau at 3.2 V, and a significant capacity (0.2 Li) is lost in agreement with earlier studies [5, 7]. It means that part of the lithium inserted during the first discharge is difficult to be deintercalated. After further cycling, the charge/discharge profiles are more similar and some extra lithium can be inserted in the phosphate due to the breaking of the particles that decreases the lithium diffusion pathway. The evolution of the discharge capacity as function of the number of cycles is shown in Fig. 7. As seen, discharge capacity is as high as 90 mAh g^{-1} at the 15th cycle, a value still not competitive for lithium ion batteries purposes. The insulating character of the iron phosphate is responsible for the reduction of a limited fraction of the iron(III) present and consequently, one mole of compound inserts less than one mole of Li. The usual methods envisaged for increasing the low electronic conductivity of the iron phosphates mostly deal with the mixing of the phosphate particles with carbon [7, 8] or ruthenium oxide [9] at intimate and microscopic level.

Sample A seems to be a mesostructure composed of amorphous $FePO_4{\cdot}2H_2O$ walls and therefore, its curve profile (Fig. 6b) looks like the one of amorphous $FePO_4{\cdot}2H_2O$. The ordered pore structure should facilitate the diffusion of lithium through the material and therefore, to increase its electrochemical activity. Other enhancing effect is the high surface area, 250 $m^2\ g^{-1}$ [10] intrinsec to mesophase, which is ten times higher than

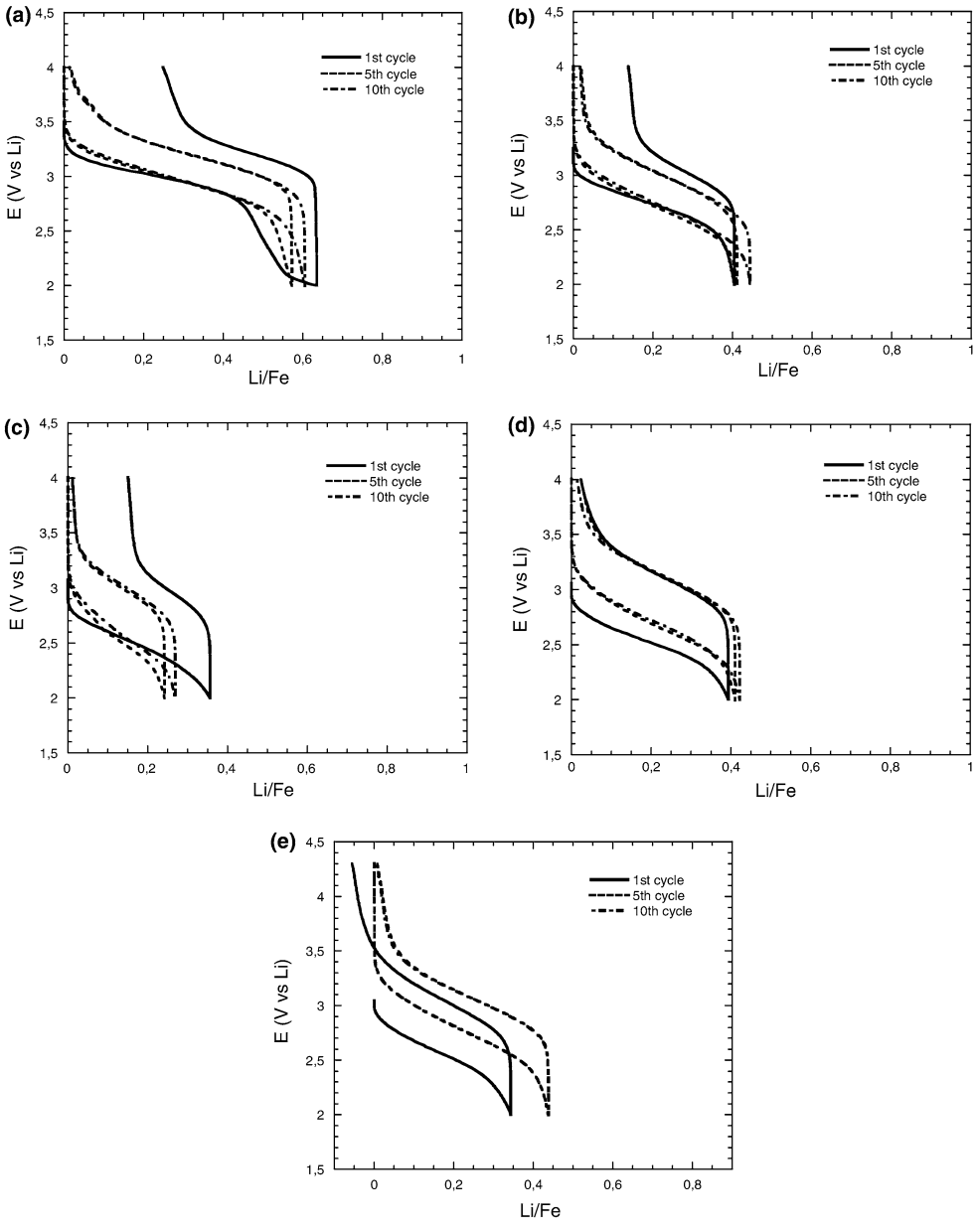

Fig. 6 First discharge/charge cycles of lithium cells in the 2.0–4.0 V range with cathode electrodes based on **a** amorphous $FePO_4{\cdot}2H_2O$, **b** sample A, **c** sample B, **d** sample C, **e** sample C tested between 2.0 V and 4.3 V

that observed for amorphous $FePO_4{\cdot}2H_2O$ [15]. It explains the lower polarisation developed by sample A cell and the smaller capacity loss during the first recharge. However, the capacity provided by the mesophase based cell is lower than for the amorphous $FePO_4{\cdot}2H_20$ cell even after further cycling since the sample A cells never provides more than 65 mAh g^{-1} (see Fig. 7). Some authors have considered as limiting factors the shape and size of the iron phosphate particles, but in our case the particles of amorphous $FePO_4{\cdot}2H_2O$ and sample A, are quite similar. Therefore, we believe that first discharge behaviour should be related to sodium acetate remaining in the galleries, therefore hindering the diffusion of the lithium by electrostatic or steric interactions.

In a first approach, samples B and C are amorphous anhydrous iron phosphates with a certain content in sodium. Prosini [4] and Whittingham [5] have reported the electrochemical activity of amorphous $FePO_4$ obtained after the heating of an amorphous hydrated sample close to 673 K. The voltage/composition curves are close to those of the hydrated systems, earlier discussed, i.e. a pseudoplateau at 3.1 V which is followed by a abrupt voltage fading close to 2.0 V, and total lithium inserted in the first discharge is $x = 0.6$ in Li_xFePO_4. Masquelier has reported a different curve profile for a composite based on carbon and 400 °C-heated amorphous $FePO_4{\cdot}1.6H_20$ [7]. For this material, a pseudoplateau with a smooth slope can be observed at 2.8 V in the range $0 < x < 0.6$ in Li_xFePO_4 and no abrupt voltage fall takes place close to 2.0 V. Both reported systems evidence that thermal treatment modifies the mechanism of the electrochemical reaction with lithium, through a

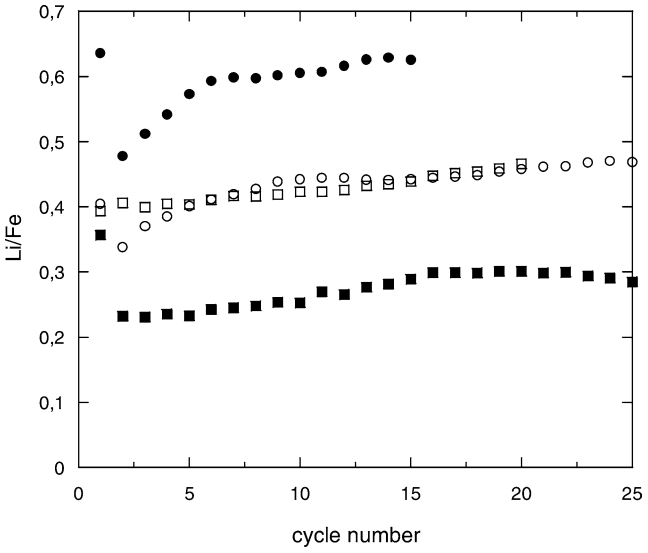

Fig. 7 Capacity versus cycle number for the lithium cells with cathode electrode based on (*filled circle*) amorphous $FePO_4{\cdot}2H_2O$, (*open circle*) sample A, (*filled square*) sample B and (*open square*) sample C

change either in the composition either in the structure of the samples. Structural water, occupying two of the octahedral coordination position of iron (III) in the amorphous $FePO_4{\cdot}2H_20$, has been considered for many research groups to solvate lithium ions and therefore, to increase the ionic conductivity of the systems [5, 7, 8]. Thermal treatment should remove this water and decrease the electrochemical performance of samples B and C. Their discharge curves are shown in Fig. 6c, d respectively. As seen, they are closer to the results reported by Masquelier although the pseudoplateau domain is smaller, $0 < x < y$ in Li_xFePO_4 ($y = 0.35$ or 0.40 for sample B and C, respectively). Small capacity discharges in the heated systems are also usually correlated to the presence of tetrahedrally coordinated iron during a process of crystallization [3, 5, 7, 8]. However the soft thermal treatment (2 h under 573 K) should not induce the crystallisation, reported to take place between 723 K and 823 K. We rather believe that particles disconnection can take place during the pyrolysis of the remaining acetate groups and the pores collapse. This phenomenon is particularly satisfactory to explain the behaviour of sample B, treated under air, since its first charge profile indicates an important loss of capacity, almost 50% of the initial one.

Sample C cell show an interesting behaviour as it recovers almost all the first charge capacity when charging and with further cycling, the cell capacity increases until 80 mAh g^{-1} at the 20th cycle. This behaviour, i.e. an almost practical reversibility of the insertion reaction, is only observed for hydrated phosphate phases, with good ionic conductivity [3–5] or for carbon coated systems, where electronic conductivity of $FePO_4$ is enhanced [7–9]. The procedure for its preparation and the black colour exhibited by sample C, indicate that we have probably coated the amorphous $FePO_4$, that built the pore walls, with a thin carbon film proceeding from the incomplete pyrolisis of organic groups. It is to be noted that the level of carbon should be so low as not detected by the TEM analyser. Nevertheless, during the thermal treatment we have also associated sodium to the amorphous structure, as its removal is possible charging to 4.3 V (Fig. 6e).

From Fig. 7, it is evident that sample A and B, provides bad cycling life or poor capacity, respectively. The good cycling performance of our sample C, in spite of

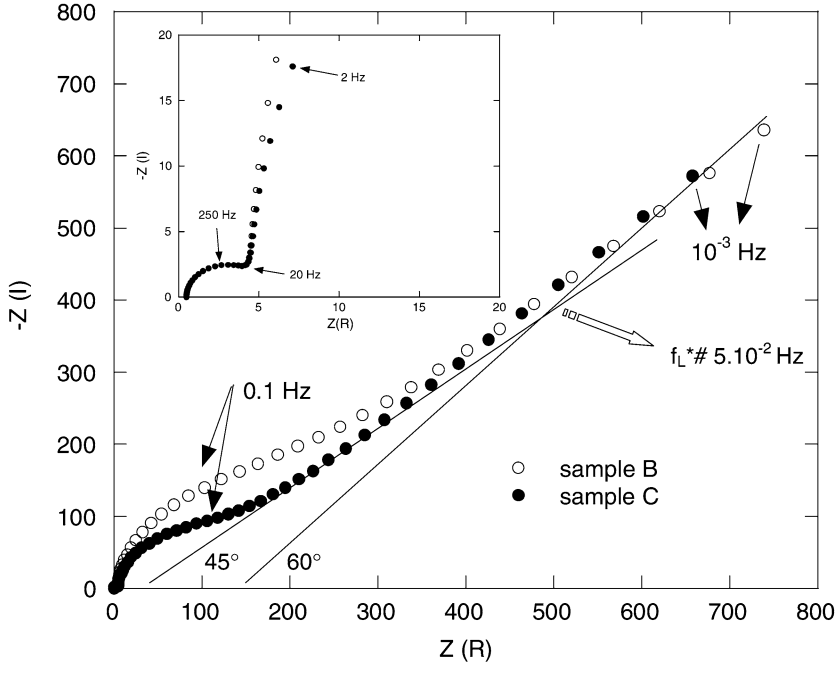

Fig. 8 EIS diagrams of sample B and sample C. Inset shows the high frequency region

the low capacity provided, gives innovative information to enhance the electrochemical properties of iron phosphate based systems. We have carried out a study of the impedance of samples B and C, in order to obtain more electrochemical parameters, and to allow us to understand their different performance. For this purpose, we have studied samples with a fixed chemical composition of $Li_{0.05}FePO_4$. The impedance diagrams are shown in Fig. 8. The electrochemical response at high frequencies (insert in Fig. 8), consists for both samples in a semicircle, which exhibits an impedance of 4Ω that could be associated to intergrain resistance. However, major differences are observed when examining the response at middle frequencies region before the apparition of a Warburg domain characterized by a slope$\{-Z'\}$ versus Z equal to 1. Indeed the values found for the charge-transfer resistance (R_{tc}) are equal to 150Ω and 80Ω for samples B and C, respectively. These impedances are related to the conductivity of the composite electrodes and, thus, to the electronic conductivity of the phosphate particles. As seen, the carbon coating efficiently improves the electronic properties of the sample C by comparison to that of sample B, allowing us to conclude that the difference in the electrochemical behaviour of each samples are related to these characteristics. Scrosati has reported a R_{tc} value of 450Ω for an anhydrous α-quartz $FePO_4$ sample [9], where iron is in tetrahedral coordination. When a coating with 5% (weight ratio) ruthenium oxide is carried out on this system, R_{tc} decreases to 260Ω, i.e. 42% lower than for pristine compound. In this context, our thermal treatment seems to be more efficient and also less expensive, considering the high cost of RuO_2. However, we must consider parameters of crystallinity, iron coordination and porosities of samples B, C and α-quartz $FePO_4$.

Finally, we have carried out an estimation of the lithium diffusion coefficient in sample C by studying, thanks to the Vaccaro's method [17], the limit frequency (f^*_L) that characterizes the end of the Warburg domain (semi-infinite diffusion) and the beginning of the capacitative region (limited diffusion, corresponding to the accumulation of lithium ions). The transition zone between both domains shows an overlapping due to two features. Firstly, the huge porosity of our electrodes, that substantially modifies the slope of the capacitative region, deviated from the theoretical 90 ° angle. Levin and Aurbach [18] have recently claimed that for porous electrodes constituted by particles with finite values of specific conductivity, the porous structure must be exactly estimated for an accurate value of the lithium diffusion coefficient. Therefore, the values calculated in this work are only approximated. Secondly, slow lithium diffusion in the phosphate based electrodes [2, 4, 19] should also explain the overlapping of the Warburg domain and the capacitative region.

Applying the formula, $D_{Li} = L^2 \times 2\pi f^*$ where L is the pathway for lithium diffusion (assimilated to a particle radium), the estimated value of D_{Li} is in the range 10^{-14} to 10^{-13} cm^2 s^{-1}. Although these values are only approximated, we can see that they are higher than that found for amorphous $FePO_4{\cdot}2H_2O$ described by Prosini [4] but are close to that reported by Franger [2] and Newman [19] on Li_xFePO_4 systems. A determination of the porous structure of our samples is now being carried out for a better discussion of their diffusion coefficients.

Conclusions

Mesoporous iron phosphate has been synthesized by a method involving the dissolution of amorphous $FePO_4{\cdot}2H_2O$ with HF, followed by the reaction with CTAB. The solid obtained, of composition $FePO_4{\cdot}(CTAB)_{0.25}{\cdot}1.7H_2O$, was submitted to extraction with sodium acetate. FTIR studies show that the resulting phase, sample A, seems to be the mesoporous variant of amorphous $FePO_4{\cdot}2H_2O$. Its electrochemical behaviour in lithium cells is characterised by a relatively low polarisation after the first discharge although the capacity is lower than for the microporous material. One promising lithium ion electrode, providing a stable capacity close to 100 mAh g^{-1}, was obtained by heating sample A at 573 K under nitrogen atmosphere. A thin film of carbon around the phosphate particles increases the electronic properties of the solid, as evidenced by impedance measurements. Major efforts are now focussed in optimizing the electrochemical performance of this electrode by increasing the carbon content.

Acknowledgements Financial support from the Spanish MCyT (Project No. MAT2002-03603) and the UIB (Project No. 2002/5) is gratefully acknowledged. JSP is grateful to UIB for supporting a short stage at LPCES/ICMMO (Orsay,France). Authors are also acknowledged to Dr. Fernando Hierro, from Serveis Cientifics of UIB, for his help in obtaining the SEM and TEM images.

References

1. Pahdi AK, Nanjundaswamy KS, Goodenough JB (1997) J Electrochem Soc 144:1188
2. Franger S, Le Cras F, Bourbon C, Rouault H (2002) Electrochem Solid State Lett 5:A231
3. Yang S, Song Y, Zavalij PY, Whittingham MS (2002) Electrochem Commun 4:239
4. Prosini PP, Lisi M, Scaccia S, Carewska M, Cardellini F, Pasquali M (2002) J Electrochem Soc 149:A297
5. Song Y, Yang S, Zavalij PY, Whittingham MS (2002) Mater Res Bull 37:1249
6. Song Y, Zavalij PY, Suzuki M, Whittingham MS (2002) Inorg Chem 41:5778
7. Masquelier C, Reale P, Wurm C, Morcrette M, Dupont L, Larcher D (2002) J Electrochem Soc 149:A1037
8. Reale P, Scrosati B, Delacourt C, Wurm C, Morcrette M, Masquelier C (2003) Chem Mater 15:5051
9. Croce F, D'Epifanio A, Settimi L, Scrosati B (2003) J Electrochem Soc 150:A576
10. Guo X, Ding W, Wang X, Yan Q (2001) Chem Commun 709
11. Nyquist RA, Kagel RO (1971) Infrared spectra of inorganic compounds, Academic, New York
12. Borras CA, Romagnoli R, Lezna RO (2000) Electrochim Acta 45:1717

13. Bellamy L (1975) The infrared spectra of complex molecules, vol 1, 3rd edn. Chapman Hall, New York
14. Wang Y-D, Ma C-L, Wui X-H, Sun X-D, Li H-D (2002) Talanta 57:875
15. Scaccia S, Carewska M, Wisniewski P, Prosini PP (2003) Mater Res Bull 8:1155
16. Scaccia S, Carewska M, Prosini PP (2004) Thermochimica Acta 413:81
17. Vaccaro AJ, Polanisamy T, Kerr RL, Maloy GT (1982) J Electrochem Soc 129:682
18. Levin MD, Aurbach D (2004) J Phys Chem B 108:11693
19. Srinivasan V, Newman J (2004) J Electrochem Soc 151:A1517